



**Period locking due to delayed feedback in a laser  
with saturable absorber**

**Thomas W. Carr**

**SMU Math Report 2002-02**

**DEPARTMENT OF MATHEMATICS  
SOUTHERN METHODIST UNIVERSITY**

## Abstract

We consider laser with saturable absorber operating in the pulsating regime that is subject to delayed optical feedback. Alone, both the saturable absorber and delayed feedback cause the CW output to become unstable to periodic output via Hopf bifurcations. The delay feedback causes the laser pulse period to lock to an integer fraction of the feedback time. We derive a map from the original model to describe the periodic pulsations of the laser. Equations for the period of the laser predict the occurrence of the different locking states as well as the value of the pump when there is a switch between the locked states.

## 1 Introduction

We consider a laser with an intracavity saturable absorber (LSA), tuned to operated in the pulsating regime, and investigate the effect of delayed-optical feedback. We find that decreased period and period-locking are the dominant effects.

Lasers with an intracavity saturable absorber (LSA) have long been used to generate high-intensity pulses (see [1, 2] for background and historical references). The effect of the absorber is to passively modulate the cavity losses so that the LSA is “self-pulsing.” The pulsed output is of practical interest for applications that require extremely short high-peak-power pulses of light. Self-pulsing semiconductor lasers (SPSL) exhibit a high repetition rate that ranges from hundreds of megahertz to a few gigahertz [3]. They are interesting for telecommunication and for optical data storage using compact disc (CD) or digital versatile disc (DVD) systems [4, 5].

Delayed-optical feedback can result from reflections off an external surface. Delayed feedback in semiconductor lasers has been successfully used for linewidth narrowing and mode selection [3]. However, the stability of the semiconductor laser’s CW output has been shown to be very sensitive to delayed optical feedback. Lang and Kobayashi [6] provided a theoretical description in the form of rate equations to describe the destabilizing effect of feedback on the laser’s CW output. Since then a large body of work has developed investigating the onset of instabilities and the progression to chaotic output referred to as “coherence collapse” (see [7] for a review). More recently, the phenomenon of LFF, or “Low-Frequency Fluctuations,” which are recurrent deep drops in the laser’s intensity, has been actively investigated (see [8] and included references).

Part of the success in using for SPSLs in CD and DVD systems is due to the fact that the self-pulsations reduce feedback-induced noise [9, 10, 11]. More recently, van Tartwijk and San Miguel [12] have numerically investigated the effect of delayed feedback in SPSLs to better quantify the statistical properties of the pulse amplitude and repetition rate due to stochastic noise. However, detailed studies of the combined deterministic dynamics of saturable absorbers and delayed feedback are limited.

In a recent study [13] we determine the conditions for the onset of oscillations and pulsations due to the presence of a saturable absorber (SA) and delay-feedback (DF). Individually, both the SA and DF cause the laser’s CW output to become unstable through Hopf bifurcations. The main result is that the SA can increase the sensitivity of the laser to DF. Or, the DF can cause self-pulsations outside the normal range of pump values for the LSA.

In the present work we investigate the effect of DF on the period and intensity of the pulses produced by the LSA. We consider a nondimensionalized model for the LSA with the addition of a delay term [14, 15, 2]:

$$\begin{aligned}\frac{dI}{dt} &= \left(D + \frac{A_2}{1 + aI} - 1\right)I + \eta I(t - \tau), \\ \frac{dD}{dt} &= \gamma[A_1 - (1 + I)D],\end{aligned}\tag{1}$$

where  $I$  is the intensity and  $D$  is the population inversion. The parameter  $\gamma$  is the inversion-decay rate normalized by the cavity-decay rate and is typically small; the strongly pulsating behavior of the LSA is directly related to the small values of  $\gamma$  [16].  $A_1$  is the pump or injected current in the case of semiconductor lasers.  $A_2 < 0$  is defined as the absorber-pump parameter and  $a$  describes the relative saturability of the absorber with respect to the active media. The feedback strength is given by  $\eta$  and delay by  $\tau$ . Eqs. (1) are commonly referred to as delay differential equations (DDE) due to the DF term.

Models for self-pulsing semiconductor lasers can include additional terms to account for nonlinear gain saturation, nonlinear damping of the active and passive regions and cross-diffusion of the carriers between active and passive regions. Also absent from our model is the linewidth enhancement factor (LWEF) or Henry parameter  $\alpha$  [17]. Including the LWEF would require that we consider the complex electric field and the evolution of the phase, which would significantly increase difficulty of our analysis. We postpone this consideration to a future work.

Self-pulsation of the LSA without feedback ( $\eta = 0$ ) appears through a bifurcation mechanism that we briefly review for the case shown in Fig. 2. The laser-first threshold occurs when  $A_1 = A_{1th} \equiv 1 - A_2$ , and the non-zero steady state (NZSS) may appear through either a supercritical or subcritical bifurcation. In Fig. 2 we show the bifurcation diagram for the subcritical case. A Hopf bifurcation to pulsating solutions appear on the non-zero branch of solutions at  $A_{1h}$  and is subcritical so that the oscillatory solutions are unstable. The oscillations become stable pulsations as the branch passes the turning point at  $A_{1hlp}$ . As  $A_1$  is decreased the oscillations become increasingly pulsating with increasing interpulse periods. The branch terminates at a homoclinic orbit of infinite period as  $A_1$  approaches  $A_{1th}$ . We note that the unstable branch of oscillatory solutions serves as a basin boundary between the NZSS and the pulsating solutions for  $A_{1h} < A_1 < A_{1hlp}$ .

## 2 Pulsing DDEs to an Map

### 2.1 Derivation of the Map

We analyze the pulsing behavior of the laser by using approximation techniques based on matched asymptotic expansions [18] to derive a map. We have previously used this method to analyze pulsations in driven class-B lasers [19] and LSAs [14]. We have also benefited from the work of Grigorieva et al. [20, 21, 22] as a guide to handling the DF. We first summarize the method before presenting the details of the map construction.

From Fig. 1 we see that the intensity is large during a very short time interval reminiscent of a boundary layer or inner solution. Following the pulse is a longer period of time where the intensity is very small corresponding to the outer solution. However, during this time there is another short time interval where the delay pulse becomes large. In each of these intervals we solve approximate equations for the laser where the terminal values from the previous interval serve as initial conditions for the next. By patching the results from one interval to the next, we determine the state of the system at  $T_1$  based on the state of the system at  $T_0$ . In general, this results in a map from  $T_n$  to  $T_{n+1}$ . Readers not interested in the details of the construction of the map can skip to the next section, Sec. 2.2.

The pulse period is typically very large with  $O(1)$  pulse widths. It is more convenient for our analysis to rescale time so that the period is  $O(1)$  while the pulse width is very small. We let  $T = \gamma t$  and obtain

$$\begin{aligned}\frac{dI}{dT} &= \frac{1}{\gamma} \left[ \left( D + \frac{A_2}{1 + aI} - 1 \right) I + \eta I (T - \tau_\gamma) \right], \\ \frac{dD}{dT} &= A_1 - (1 + I)D,\end{aligned}\tag{2}$$

where  $\tau_\gamma = \gamma\tau$ .

$T \in [T_0, T'_0]$ : The time  $T = T_0$  and  $T = T'_0$  as the start and end of the present pulse; in general,  $T_n$  and  $T'_n$  are the start and end of pulses  $n = 1, 2$ , etc. During the first pulse the intensity is very large  $I(T) \gg 1$  and we assume the delayed pulse has not yet been re-injected into the laser and is small,  $I(T - \tau_\gamma) \ll 1$ . The LSA equations are approximated as

$$\frac{dI}{dT} = \frac{1}{\gamma} (D - 1)I, \quad \frac{dD}{dT} = ID,\tag{3}$$

These can be solved in the phase plane by determining the equation for  $dI/dD$  whose solution is

$$I(T) - I(T_0) = \frac{1}{\gamma} \left[ -(D(T) - D(T_0)) + \ln \left( \frac{D(T)}{D(T_0)} \right) \right].\tag{4}$$

The time  $T'_0$  is defined as when the intensity has returned to its initial value,  $I(T'_0) = I(T_0)$ . Thus, the inversion evolves during the pulse according to

$$0 = -[D(T'_0) - D(T_0)] + \ln \left( \frac{D(T'_0)}{D(T_0)} \right).\tag{5}$$

$T \in [T'_0, T_0 + \tau_\gamma]$ : The next interval from  $T = T'_0$  to  $T = T_0 + \tau_\gamma$  is when both the intensity and the delayed intensity are small;  $I(T) \ll 1$  and  $I(T - \tau_\gamma) \ll 1$ . On this interval we solve

$$\frac{1}{I} \frac{dI}{dT} = \frac{1}{\gamma} (D + A_2 - 1), \quad \frac{dD}{dT} = A_1 - D,\tag{6}$$

with initial conditions  $I(T'_0) = I(T_0)$  and  $D(T'_0) = D(T'_0)$  that are determined by the terminal values of the previous interval. The equation for  $D$  can be solved first and the result used

to solve for  $I$ . The solutions are

$$\begin{aligned} D(T_0 + \tau_\gamma) &= A_1 + (D(T'_0) - A_1)e^{-(T_0 + \tau_\gamma - T'_0)}, \\ \gamma \ln\left(\frac{I(T_0 + \tau_\gamma)}{I(T_0)}\right) &= [A_1 - (1 - A_2)](T_0 + \tau_\gamma - T'_0) - (D(T'_0) - A_1)(e^{-(T_0 + \tau_\gamma - T'_0)} - 1). \end{aligned} \quad (7)$$

$T \in [T_0 + \tau_\gamma, T'_0 + \tau_\gamma]$ : The effect of the delayed pulse occurs during the interval  $T = T_0 + \tau_\gamma$  to  $T = T'_0 + \tau_\gamma$  when  $I(T) \ll 1$  but  $I(T - \tau_\gamma) \gg 1$ . On this interval we solve

$$\frac{dI}{dT} = \frac{\eta}{\gamma} I(T - \tau_\gamma), \quad \frac{dD}{dT} = A_1 - D, \quad (8)$$

with initial conditions  $I(T_0 + \tau_\gamma)$  and  $D(T_0 + \tau_\gamma)$ . Each equation can be solved independently to give

$$\begin{aligned} D(T'_0 + \tau_\gamma) &= A_1 + (D(T_0 + \tau_\gamma) - A_1)e^{-(T'_0 - T_0)}, \\ I(T'_0 + \tau_\gamma) - I(T_0 + \tau_\gamma) &= \frac{\eta}{\gamma} \int_{T_0}^{T'_0} I(T - \tau_\gamma) dT = \frac{\eta}{\gamma} p. \end{aligned} \quad (9)$$

The effect of the delay is to cause a jump in the intensity proportional to the area of the original pulse. The latter can be thought of as the energy in the pulse. If there is no feedback ( $\eta = 0$ ), there is effectively no change in the intensity over the very small time interval defined by the width of the pulse.

$T \in [T'_0 + \tau_\gamma, T_1]$ : Finally, the last time interval is from the end of the delayed pulse,  $T = T'_0 + \tau_\gamma$  to the start of the next real pulse at  $T = T_1$ . The time  $T_1$  is defined as when the intensity is equal to that at the start of the preceding pulse, i.e.,  $I(T_1) = I(T_0)$ . Both the pulse and the delayed pulse are small and we solve the same equations as during  $T \in [T'_0, T_0 + \tau_\gamma]$ . We find that

$$\begin{aligned} D(T_1) &= A_1 + (D(T'_0 + \tau_\gamma) - A_1)e^{-(T_1 - T'_0 - \tau_\gamma)}, \\ \gamma \ln\left(\frac{I(T_0)}{I(T'_0 + \tau_\gamma)}\right) &= [A_1 - (1 - A_2)](T_1 - T'_0 - \tau_\gamma) - (D(T'_0) - A_1)(e^{-(T_1 - T'_0)} - e^{-\tau_\gamma}) \end{aligned} \quad (10)$$

## 2.2 The Map

The map is determined by finding a relationship for  $D(T_1)$  and  $T_1$  in terms of  $D(T_0)$  and  $T_0$ . These values of  $D_n = D(T_n)$ ,  $n = 0, 1, 2, \dots$  correspond to the maximum of the population inversion. The minimum values of the inversion are given by  $G_n = D(T'_n)$ ,  $n = 0, 1, 2, \dots$ . In constructing the map we use the fact that the width of the pulse in the timescale  $T$  is  $O(\gamma)$  and thus can be ignored. Also, the times  $T_n$  are defined by when the intensity reaches a fixed value, which for algebraic convenience we set such that  $I(T_n) = I(T_0) = 1$ . (Analysis of the map shows that  $dP/dI(T_0) = O(\gamma)$ . That is, changing the value of the intensity that is used as the starting point of the pulse causes only small changes in the period.) After eliminating as many intermediate variables as possible, the map is given by

$$D_{n+1} = A_1 + (G_n - A_1)e^{-P_n}, \quad (11)$$

$$T_{n+1} = T_n + P_n, \quad (12)$$

$$0 = \ln\left(\frac{G_n}{D_n}\right) - (G_n - D_n), \quad (13)$$

$$\frac{\eta}{\gamma} p_n = e^{C_1} - e^{C_2}, \quad (14)$$

$$D_n - p_n = D_n e^{-p_n}, \quad (15)$$

$$C_1 \gamma = -\lambda(P_n - \tau_\gamma) + (G_n - A_1)(e^{-P_n} - e^{-\tau_\gamma}), \quad (16)$$

$$C_2 \gamma = \lambda \tau_\gamma + (G_n - A_1)(1 - e^{-\tau_\gamma}), \quad (17)$$

$$\lambda = A_1 - A_{1th} = A_1 - (1 - A_2). \quad (18)$$

The effect of the delay is accounted for by the variable  $p_n$  defined in Eq. (9). However, instead of computing this integral we follow the approach in [20, 21, 22]; We use Eq. (3) in the pulse interval  $T \in [T_0, T'_0]$  to determine Eq. (15) above.

The map in Eq. (11)-(18) assumes that the delay pulse occurs before the next pulse, i.e.,  $\tau_\gamma < P_n$ . These are referred to as “slowly oscillating” (SO) solutions by Grigorieva et al. [20, 21, 22]. For longer delays there may be two or more pulses per delay interval; these are referred to as “fast oscillating” (FO) solutions. For FO solutions, if  $P_n < \tau_\gamma < P_n + P_{n-1}$ , then the pulse at  $T_{n-1}$  effects the evolution from  $T_n$  to  $T_{n+1}$ . For a given  $\tau_\gamma$  it may be the pulse starting at  $T_{n-m}$  that effects the present interval starting at  $T_n$ .

The method to construct the map for FO solutions is the same as for SO solutions under the assumption that the energy in the previous pulses,  $p_{n-m}, p_{n-m+1}, \dots, p_{n-1}$ , and the time intervals between them,  $P_{n-m}, P_{n-(m+1)}, \dots, P_{n-1}$ , are known.

$$D_{n+1} = A_1 + (G_n - A_1)e^{-P_n}, \quad (19)$$

$$T_{n+1} = T_n + P_n, \quad (20)$$

$$0 = \ln\left(\frac{G_n}{D_n}\right) - (G_n - D_n), \quad (21)$$

$$\frac{\eta}{\gamma} p_{n-m} = e^{C_1} - e^{C_2}, \quad (22)$$

$$D_n - p_n = D_n e^{-p_n}, \quad (23)$$

$$C_1 \gamma = -\lambda(P_n - \xi_n) + (G_n - A_1)(e^{-P_n} - e^{-\xi_n}), \quad (24)$$

$$C_2 \gamma = \lambda \xi_n + (G_n - A_1)(1 - e^{-\xi_n}), \quad (25)$$

$$\xi_n = \begin{cases} \tau_\gamma - \sum_{j=1}^m P_{n-j}, & m \geq 1 \\ \tau_\gamma, & m = 0. \end{cases} \quad (26)$$

The map determines the next value of inversion  $D_{n+1}$  and time  $T_{n+1}$  in terms of previous values as defined by Eqs. (19) and (20). The delay is accounted for by the variable  $p_{n-1}$  corresponding to the energy of the pulse at  $T_{n-m}$ . Likewise,  $\tau_\gamma$  has been replaced by  $\xi_n$  defined by Eq. (26). The FO map reduces to the SO map when  $m = 0$ . Hence, our attention will focus on Eqs. (19)-(26) for further analysis.

### 3 Periodic Pulsations

One motivation for deriving a map is that iterating the map is typically much easier and quicker than numerically simulating the original flow from which it was derived. In the present case, however, the map consists of nonlinear, coupled implicit equations that are very difficult to solve. Transient or chaotic behavior is better simulated using the original differential equation. Instead, we will examine periodic solutions that correspond to fixed points of the map. The resulting equations are still difficult to solve but with further approximations we will obtain excellent results.

As stated above, fixed points of the map correspond to periodic solutions of the original system. Thus, all variables (except for time) are constants independent of the index  $n$ .

$$D = A_1 + (G - A_1)e^{-P}, \quad (27)$$

$$T_{n+1} = T_n + P, \quad (28)$$

$$0 = \ln\left(\frac{G}{D}\right) - (G - D), \quad (29)$$

$$\frac{\eta}{\gamma}p = e^{C_1} - e^{C_2}, \quad (30)$$

$$D - p = De^{-p}, \quad (31)$$

$$C_1\gamma = -\lambda(P - \xi) + (G - A_1)(e^{-P} - e^{-\xi}), \quad (32)$$

$$C_2\gamma = \lambda\xi + (G - A_1)(1 - e^{-\xi}), \quad (33)$$

$$\xi = \tau_\gamma - mP, \quad m = 0, 1, 2, \dots \quad (34)$$

Equation (30) for the period  $P$  can be written as

$$\frac{\eta}{\gamma}p = e^{C_1} \{1 - \exp[\frac{1}{\gamma}(\lambda P + (G - A_1)(1 - e^{-P}))]\} \quad (35)$$

The right hand side must be positive because it represents the energy of the pulse. Thus, the exponent of the exponential of the right hand side must be negative, or,

$$\lambda P + (G - A_1)(1 - e^{-P}) < 0. \quad (36)$$

This equation, when made an equality, is exactly the equation for the LSA's natural period without DF (see [14] without modulation). Thus, the inequality restricts the period of the laser with delayed feedback to be less than that of the unperturbed laser without feedback ( $\eta = 0$ ). The condition imposed by Eq. (36) suggests our first approximation.

**Approximation A1:** Assume that the period is bound away from and below the  $\eta = 0$  curve. Specifically, assume that the  $\exp[\cdot]$  term on the right-hand side is small. Then the equation for the period reduces to  $C_1(P) = \ln(\frac{\eta}{\gamma}p)$ .

The approximation A1 is undefined for  $\eta = 0$  and we expect that subsequent results will be singular in this limit. To properly examine the case of  $\eta p/\gamma \rightarrow 0$  requires that the contribution of the  $(1 - \exp(C_2 - C_1))$  be included.

**Approximation A2:** Our second approximation applies to the Eq. (29) for  $G$ , the minimum of the population inversion. For pulsating solutions the minimum is very close to zero. Thus,  $G \ll |\ln G|$  in Eq. (29) leading to the approximation  $G \approx De^{-D}$ , which fits Eq. (29) for even moderate values of  $D$ . For physically realistic values of  $D$ , say  $D > 3.5$ , we can take  $G \approx 0$ .

**Approximation A3:** Assume the energy in the pulses is large enough so that  $\exp(-p) \ll 1$ . Then  $p \approx D$ . Again, this approximate result fits Eq. (31) well for reasonable values of  $D$ .

Applying approximations A1, A2 and A3 to the steady-state conditions results in a single equation for the period that can then be used to determine the inversion.

$$\lambda(P - \xi) + A_1(e^{-P} - e^{-\xi}) = -\gamma \ln\left[\frac{\eta}{\gamma} A_1(1 - e^{-P})\right], \quad (37)$$

$$D = A_1(1 - e^{-P}). \quad (38)$$

A numerical solution for the period  $P$  is now much easier to obtain than if we had used the original fixed-point equations. However, we can obtain explicit results for  $P$  with two additional approximations.

**Approximation A4:** Suppose that  $P - \xi = (m + 1)P - \tau_\gamma \ll 1$ . We refer to this as the locking approximation because the laser period is an integer multiple of the delay. To find  $P$  we let  $P = (\tau_\gamma + P_1)/(m + 1)$  where  $P_1 \ll 1$ . The result is

$$\text{A4: } P = \frac{\tau_\gamma}{m + 1} - \frac{\gamma}{m + 1} \frac{\ln\left[\frac{\eta}{\gamma} A_1(1 - e^{-\frac{\tau_\gamma}{m+1}})\right]}{[A_1(1 - e^{-\frac{\tau_\gamma}{m+1}}) - A_{1th}]}, \quad (39)$$

where we have dropped an  $O(\gamma)$  term in the denominator of the correction. We will refer to the locking approximation for  $P$  in Eq. (39) as A4.

**Approximation A5:** If the lasers are not locked the period is typically large enough so that  $e^{-P} \ll 1$ . Also, in general, we need only consider the case  $m = 0$  because when  $m \geq 1$  the solutions are locked and better described by A4.

$$\text{A5: } P = \tau_\gamma + \frac{A_1}{\lambda} e^{-\tau_\gamma} - \frac{\gamma}{\lambda} \ln\left[\frac{\eta}{\gamma} A_1\right] \quad (40)$$

We will refer to this “unlocked” result for the period, Eq. (40), as A5.

We note that  $P = A_1/\lambda$  ( $\lambda = A_1 - A_{1th}$  by Eq. (18)) is the  $P \gg 1$  approximation to the LSA’s natural period without DF ( $\eta = 0$ ) (see [14] or Eq. (36) with  $P \rightarrow 0$  and  $G \approx 0$ ). If  $\tau_\gamma \rightarrow 0$ , the feedback term in the DDEs Eq. (1) becomes a modification to the linear dissipation. This modifies the period through the natural log term in the equation above. Also, the results of A4 and A5 are equivalent in the limit  $\tau_\gamma \rightarrow \infty$  ( $m = 0$ ).

## 4 Period Locking

The analytical approximations derived in the previous section can be used to determine the period as a function of the pump,  $P(A_1)$ . We will compare the analytical results from the map (shown as solid curves in the figures) to the results of numerically simulating the original DDEs (shown as dashed lines). We used the MATLAB routine DDE23 [23] to numerically integrate Eq. (1) rewritten in terms of the electric field, where  $I = |E|^2$ . The latter is done to avoid accuracy problems resulting from the high-amplitude pulsations. We will first present results for long delays where period locking occurs, followed by short delays that do not exhibit locking. Finally, the intermediate regime that exhibits characteristics of both will be discussed.

### 4.1 Long Delay: Locked Period

We begin with the case of  $\tau = 50$  in Fig. 3a; the solid lines are due to the map while the dashed lines are due to direct simulation of the DDEs. The upper-dashed curve is the natural period of the LSA when there is no DF ( $\eta = 0$ ). As the pump decreases to the threshold value,  $A_1 \rightarrow A_{1th}$ , the system approaches a homoclinic orbit and the period becomes unbounded. As the pump is increased so that  $A_1 \rightarrow A_{1hlp}$ , the period decreases to a finite value. The nearby solid curve results from the map for the case  $\eta = 0$  and fits the numerical result very well.

The stepped-dashed curve in Fig. 3a is the period of the laser determined by numerical simulation of the DDEs with DF ( $\eta \neq 0$ ). When the pump is near threshold the laser locks to a period determined by the delay,  $P \approx \tau$ . As the pump is increased the period approaches that of the LSA's natural period. Before exceeding the natural period, the laser's period jumps down to a new locked value of  $P \approx \tau/2$ .

The left-most solid curve is the analytical approximation of the period from A5. For values of the pump close to threshold  $A_1 \rightarrow A_{1th}$  so  $\lambda \rightarrow 0$  and A5 is dominated by the  $A_1/\lambda$  term. As the pump is increased the period quickly asymptotes to the locked state  $P \approx \tau$  ( $m = 0$ ). As the pump is increased the value predicted by A5 intersects with the natural period of the LSA. At this point we use the lowest solid curve for the period determined by the approximation A4, where  $P \approx \tau_\gamma/2$  ( $m = 1$ ).

As stated above, the switch of the laser period from one locked state to another is determined by the LSA's natural period. That is, the maximum period the laser can support is the natural period of the LSA determined by the LSA parameters. Theoretically, this condition is provided by examining the asymptotic validity of the map. The interval  $T \in [T'_0, T_0 + \tau_\gamma]$  is the time after the end of the pulse and before the delayed pulse becomes large. That is, both  $I(T) \ll 1$  and  $I(T - \tau_\gamma) \ll 1$  on this interval. However, the pulse grows exponentially on this interval according to Eq. (7). At first, the net increase is very small. However, it will eventually become large enough to initiate the next pulse at  $T_1$ . For the map construction to remain valid we require that the delayed pulse occurs before the intensity starts to grow. This will be true if the right-hand side of Eq. (7) remains negative on the interval. To analyze this condition we consider its more general analog for the FO map, assume periodic solutions, and let  $G \approx 0$  (the minimum of the inversion) according to

approximation A2. We have then that

$$\lambda(\tau_\gamma - mP) - A_1(1 - e^{-(\tau_\gamma - mP)}) < 0. \quad (41)$$

For both locked and unlocked periodic solutions ( $(m + 1)P - \tau \approx 0$ ,  $m \geq 1$  and  $m = 0$ , respectively) the condition imposes a constraint on the pump for each value of  $m$ :

$$A_1 < \frac{cA_{1th}}{c - 1}, \quad c = \frac{\frac{\tau_\gamma}{m+1}}{1 - e^{-\frac{\tau_\gamma}{m+1}}} \quad (42)$$

The values of  $A_1$  where (42) is satisfied as an equality define the switching point from  $m$  to  $m + 1$ . This is indicated by the thick solid line at  $A_1 = 7.1$  in Fig. 3a.

As a additional demonstration of period locking, Fig. 4 shows the case of  $\tau = 100$ . Because the period is longer the period locking phenomena is even more dramatic. In this case the lock states correspond to  $P \approx 100, 50, 33, 25$  for  $m = 0, 1, 2, 3$ , respectively. We again see an excellent fit between numerical results and the map's prediction for the period. The switch point for each solution is again indicated by thick solid lines.

As has been demonstrated, the period of the laser in the presence of DF is determined by the delay time  $\tau$ . The strength of the feedback  $\eta$  modifies the period  $P$  through the  $O(\gamma)$  correction terms and, hence, has a small effect. In Fig. 5 we have plotted the period  $P$  as a function of the feedback strength  $\eta$  for two different values of the pump. In Fig. 5a, we compare numerical results (dashed) to the analytical result (solid) of A4 (period locking), while in Fig. 5b, we compare to A5 (decaying period). The dotted curves are shifted versions of the analytical result so that the slopes of the numerical and analytical results can be visually compared. In both cases there is a very good fit except for when the feedback strength  $\eta$  is small. The analytical results determine that  $dP/d\eta \propto 1/(\eta\lambda)$ ; the slope of the  $P$  vs.  $\eta$  curve decreases for increasing  $\eta$ . However, the limit  $\eta \rightarrow 0$  is singular and would require a more precise analysis to achieve better fit in this regime.

## 4.2 Short Delay: Unlocked Period

Figure 6 shows the case of short delay,  $\tau = 2$  such that the LSA's natural period is always greater than the delay time. Hence, no locking will occur until possibly very large pump when the period is low. The dashed curve in both Figs. 6a and b is the result of numerical simulation of the DDEs for the laser with DF. The LSA's natural period is shown by the dotted line to more easily distinguish it from the case with DF.

The analytical result A5 is shown in Fig. 6a. A5 was derived with the approximation  $P \gg 1$  and for large period A5 follows the result of numerical simulation quite well. However, it loses some fidelity for small period (large pump). This error is due to the large period approximation used to derive A5 rather than an intrinsic difficulty of the map. In Fig. 6b we show the result of numerically solving the map equation for the period after approximation A3. Here, the map result follows the numerical result extremely well even for large pump.

## 4.3 Moderate Delay

For long delays we see that the period locks to a fraction of the delay time, while for short delays the period is a perturbation of the natural LSA period approximated by  $P = A_1/\lambda$ .

Moderate delays show both of these characteristics. Fig. 7 is the case of  $\tau = 20$ . For pump values not far from threshold the period decays. Then, near  $A_1 \approx 5.9$  the period drops to the vicinity of  $P \approx \tau$ . As the pump increases further, the period becomes more closely locked. The drop in the period is not a switch between two intervals of locked period, say  $m = 0$  in  $m = 1$ . It occurs when the delay is long enough so that the trailing edge of the pulse  $I(t - \tau)$  begins to overlap with the leading edge of the next pulse of  $I(t)$ . Our analysis is not yet refined enough to capture the phenomena.

The map result A5 captures the decaying period for low pump but asymptotes to a value that is too large. However, A4 ( $m = 0$ ), which is more appropriate for when the period is locked, gives a reasonable fit. The main difference is due to the terms  $\exp(-\tau/\gamma)$  in A4 which are significant for lower values of delay time.

#### 4.4 Maximum Pulse Intensity

The maximum intensity of the pulses is an important design quantity that can also be determined from the map. The pulse occurs during the initial time interval  $T \in [T_0, T'_0]$ . The maximum occurs when  $dI/dT = 0$  and so from Eq. (3) this requires  $D = 1$ . The latter is substituted in Eq. (4) to obtain a formula for the maximum pulse intensity in terms of the initial value of the inversion, which in the map is  $D_n$ . For periodic solutions, the inversion is found from the period with Eq. (38) so that we have

$$I_{\max} = \frac{1}{\gamma} [A_1(1 - e^{-P}) - 1 - \ln(A_1(1 - e^{-P}))], \quad (43)$$

where we have kept only the large  $O(1/\gamma)$  terms. The maximum intensity is affected by the delay through the period  $P$ . The equations used to derive Eq. (43) are the same whether delay is considered or not. That is, the maximum intensity depends on the period of the pulsations and only indirectly on the delay, which affects the period. It might be tempting to also ignore the small  $e^{-P}$  terms. However, the effect of the delay would then be absent from the result.

In Fig. 3b we compare the analytical and numerical results for the pulse amplitude when  $\tau = 50$ . Eq. (42) again predicts the value of the pump when the switch from one lock state to another occurs.

## 5 Discussion

Finally, if there is no delayed feedback  $\eta = 0$  and the map, Eqs. (19)-(26), reduces to the map derived by us in [14] when there is no modulation. This, at least, is a check on the consistency of our result.

There are two transition regions where more detailed and specialized analysis is warranted. The first is the transition between different locked regions, for example, the transition from  $m = 0$  to  $m = 1$ . When  $m = 0$  the effect of the delayed pulse occurs before the second pulse is emitted, while for  $m = 1$  the effect of the delay pulse occurs after the second pulse but before the third. Our analysis assumes that the real and delayed pulse occur in

non-overlapping time intervals. However, the transition between locked states occurs when the period is nearly an multiple of the delay so that there is overlap between the next pulse and the delayed pulse. A second type of transition occurs for intermediate delays like the case  $\tau = 20$ . Here we had a jump down from an exponential decaying period to a locked period for  $m = 0$ . Here again, this transition occurs as the delayed pulse interval overlaps with the next pulse. Analysis of these transition will require reexamining inner regions in the matched asymptotics construction of the map.

## 6 Acknowledgments

This work was supported by the National Science Foundation Grant No. DMS-9803207.

## References

- [1] A.E. Siegman. *Lasers*. Univ. Science Books, 1986.
- [2] P. Mandel. *Theoretical Problems in Cavity Nonlinear Optics*. Cambridge Studies in Modern Optics. Cambridge University Press, New York, 1997.
- [3] G.P. Agrawal and N.K. Dutta. *Long-Wavelength Semiconductor Lasers*. Reinhold, New York, 1986.
- [4] M. Yamada. A theoretical analysis of self-sustained pulsation phenomena in narrow-stripe semiconductor lasers. *IEEE J. Quantum Electron.*, 29:1330–1336, 1993.
- [5] D.R. Jones, P. Reese, I. Pierce, and H.D. Summers. Theoretical optimization of self-pulsating 660-nm wavelength AlGaInP laser disodes. *IEEE Journal of Selected Topics in Quantum Electronics*, 5:740–744, 1999.
- [6] R. Lang and K. Kobayashi. External optical feedback effects on semiconductor injection laser properties. *IEEE J. Quantum Electron.*, QE-16:347–355, 1980.
- [7] G.H.M. van Tartwijk and D. Lenstra. Semiconductor lasers with optical injection and feedback. *Quantum Semiclass. Opt.*, 7:87–143, 1995.
- [8] A. Gavrielides, T.C. Newell, V. Kovanis, R.G. Harrison, N. Swanston, Dejin Yu, and Weiping Lu. Synchronous sisyphus effect in diode lasers subject to optical injection. *pra*, 60:1577–1581, 1999.
- [9] S. Matsui, H. Takiguchi, H. Hayashi, S. Yamamoto, S. Yano, and T. Hijikata. Suppression of feedback induced noise in short V-channel substrate inner-stripe lasers with self-pulsations. *Appl. Phys. Lett.*, 43:219–221, 1983.

- [10] Y. Simler, J. Gamelin, and S. Wang. Pulsation stabilization and enhancement in self-pulsating laser diodes. *IEEE Photon. Technol. Lett.*, 4:329–332, 1992.
- [11] E.A. Avrutin. Analysis of spontaneous emission and noise in self-pulsing laser diodes. *Proc. Inst. Elect. Eng.*, 140:16–20, 1993.
- [12] G.H.M. van Tartwijk and M.S. Miguel. Optical feedback on self-pulsing semiconductor lasers. *IEEE J. Quantum Electron.*, 32:1191–1202, 1996.
- [13] T.W. Carr. Onset of instabilities in self-pulsing semiconductor lasers with delayed feedback. *Euro. Phys. J. D.*, 19:245–255, 2002.
- [14] T.W. Carr and T. Erneux. An analytical study of a periodically driven laser with a saturable absorber. *Euro. Phys. J. D.*, 17:67–74, 2001.
- [15] T.W. Carr and T. Erneux. Dimensionless rate equations and simple conditions for self-pulsing in laser diodes. *IEEE J. Quantum Electron.*, 37:1171–1177, 2001.
- [16] T. Erneux. Q-switching bifurcation in a laser with a saturable absorber. *J. Opt. Soc. Am. B*, 5:1063–1069, 1988.
- [17] C.H. Henry. Theory of the linewidth of semiconductor lasers. *IEEE J. Quantum Electron.*, QE-18, 1982.
- [18] J. Kevorkian and J.D. Cole. *Multiple Scale and Singular Perturbation Methods*. Springer-Verlag, New York, 1996.
- [19] T.W. Carr, L. Billings, I.B. Schwartz, and I. Triandaf. Bi-instability and the global role of unstable resonant orbits in a driven laser. *Physica D*, 147:59–82, 2000.
- [20] E.V. Grigorieva, S.A. Kahchenko, N.A. Loiko, and A.M. Samson. Nonlinear dynamics in a laser with negative delayed feedback. *Physica D*, 59:297–319, 1992.
- [21] E.V. Grigorieva and S.A. Kashchenko. Regular and chaotic pulsations in laser diode with delayed feedback. *Int. J. of Bifurcation and Chaos*, 3:1515–1528, 1993.
- [22] E.V. Grigorieva. Complex temporal structures in models of a laser with optoelectronic delayed feedback. *Optics Commun.*, 102:182–192, 1993.
- [23] L.F. Shampine and S. Thompson. Solving ddes in Matlab. *J. Appl. Numer. Math.*, 37:441–458, 2001. See also <http://www.cs.runet.edu/thompson/webddes/index.html>.
- [24] E.J. Doedel, A.R. Champneys, T.F. Fairgrieve, Y.A. Kuznetsov, B. Sandstede, and X. Wang. Auto97: Continuation and bifurcations software for ordinary differential equations (with homcont). <http://indy.cs.concordia.ca/auto>.

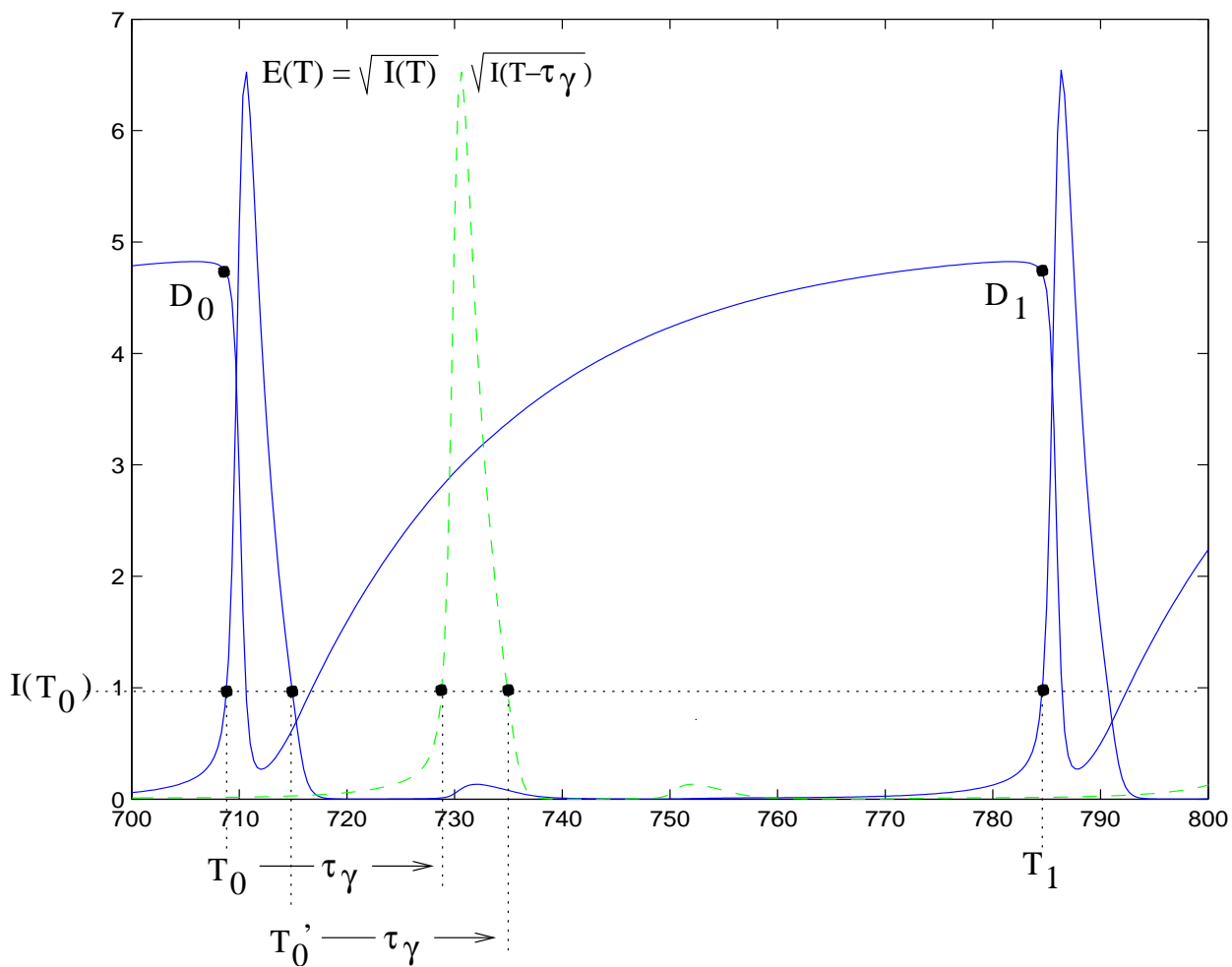


Figure 1: For two subsequent pulses the map variables  $T_n$  and  $D_n$  are shown. The electric field, equal to the square root of the intensity, is plotted so that its magnitude is comparable to the inversion and they can be seen on the same graph. The time delayed pulse is shown as a dashed line.

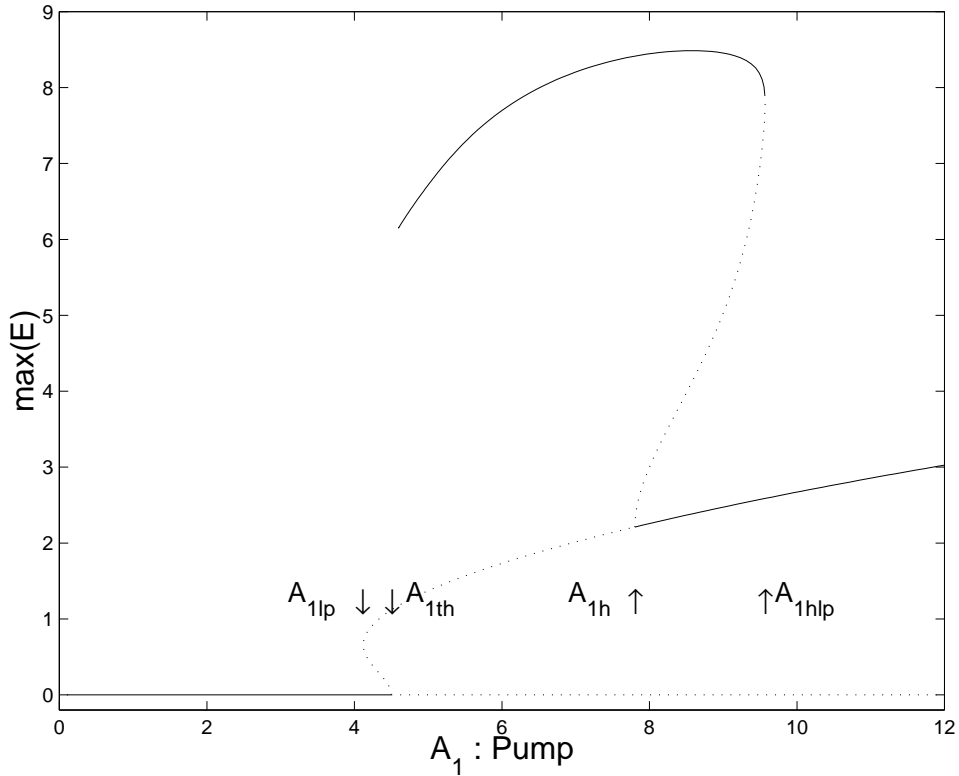


Figure 2: Bifurcation diagram [24] of the LSA without feedback ( $\eta = 0$ ). Solid/dotted lines are stable/unstable solutions, respectively.  $A_{1th} = 4.5$  is the bifurcation of the zero steady state to the non-zero steady state.  $A_{1lp} = 4.1$ .  $A_{1h} = 7.8$  is the Hopf bifurcation to periodic solutions that are unstable. Pulsating solutions occur on the upper branch between  $A_{1hlp} = 9.6$  and  $A_{1th}$ , where they terminate in a homoclinic orbit ( $A_2 = -3.5$ ,  $a = 2$ ,  $\gamma = 0.05$ ).

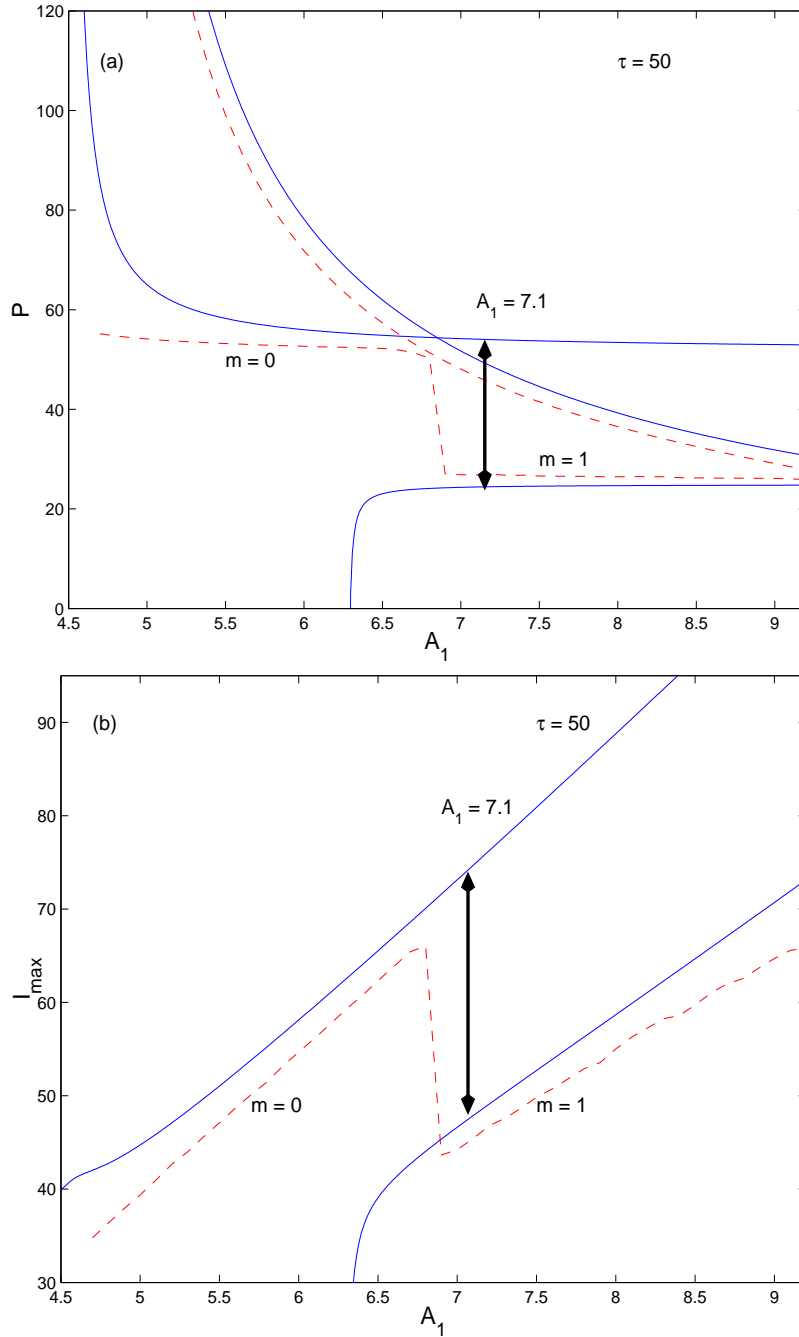


Figure 3: In both (a) and (b) solid curves correspond to analytical results while the dashed curves are from numerical simulations. (a) Period vs. pump. The right most decaying curves are for the case of no DF,  $\eta = 0$ . The map predicts the blow-up of the period as  $\lambda \rightarrow 0$  and the homeclinic orbit is approached. In the presense of DF ( $\eta \neq 0$  there is exponential decay of the period until it locking.  $A_1 \approx 7.1$  is the analytical prediction of the switching point between the  $m = 0$  curve and the  $m = 1$  curve when the pump is increased or decreased. (b) As the pump is increased the intensity of the pulses increases as the period decreases (from (a)). At the switch point the intensity abrubly decreases and then follows the new branch of solutions for increasing pump.

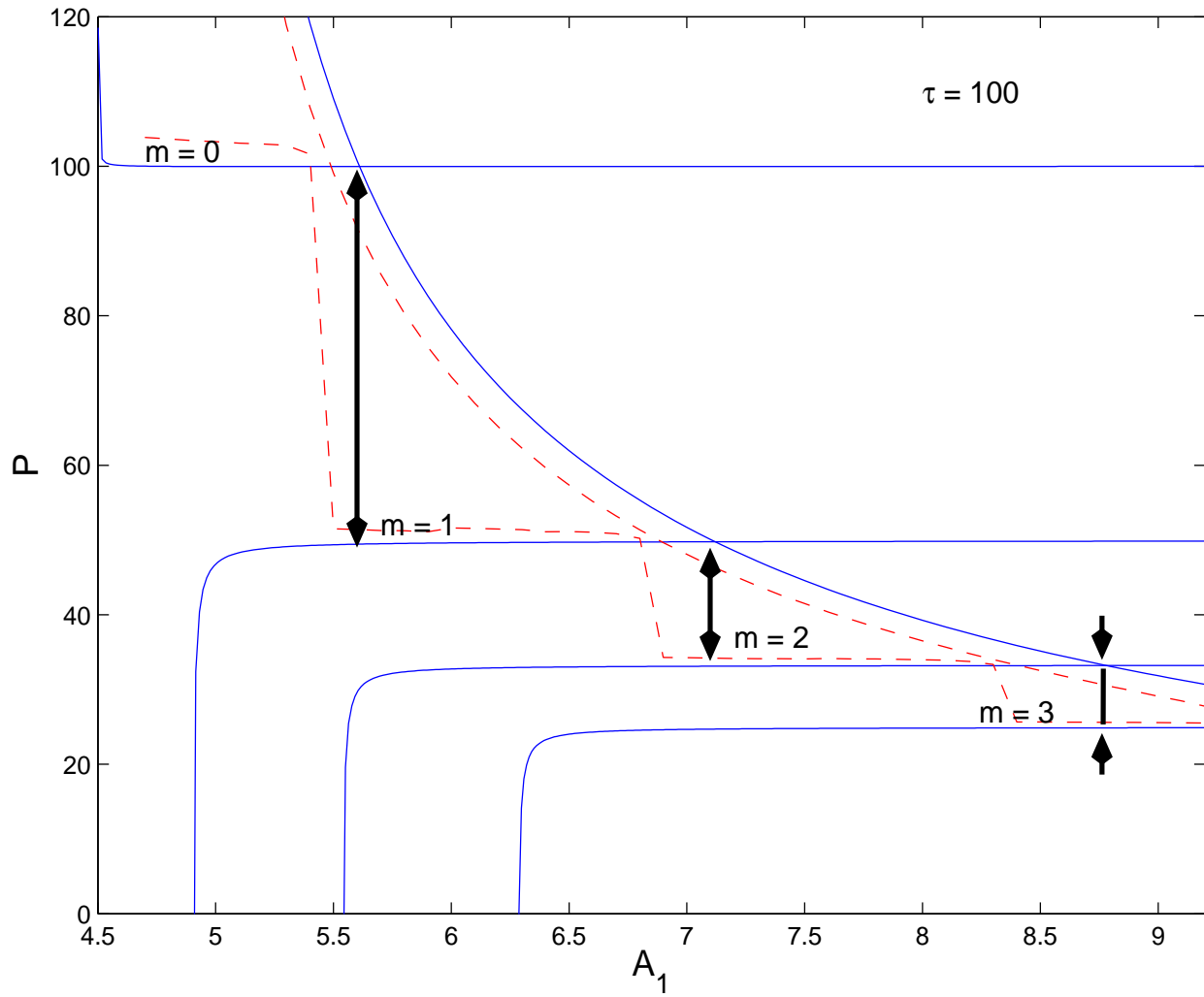


Figure 4: Large delay allows for more locking regions,  $P \approx \tau_\gamma / (m+1)$ . Analytical predictions for the switch points are indicated. Solid curves = analytical, dashed = numerical.

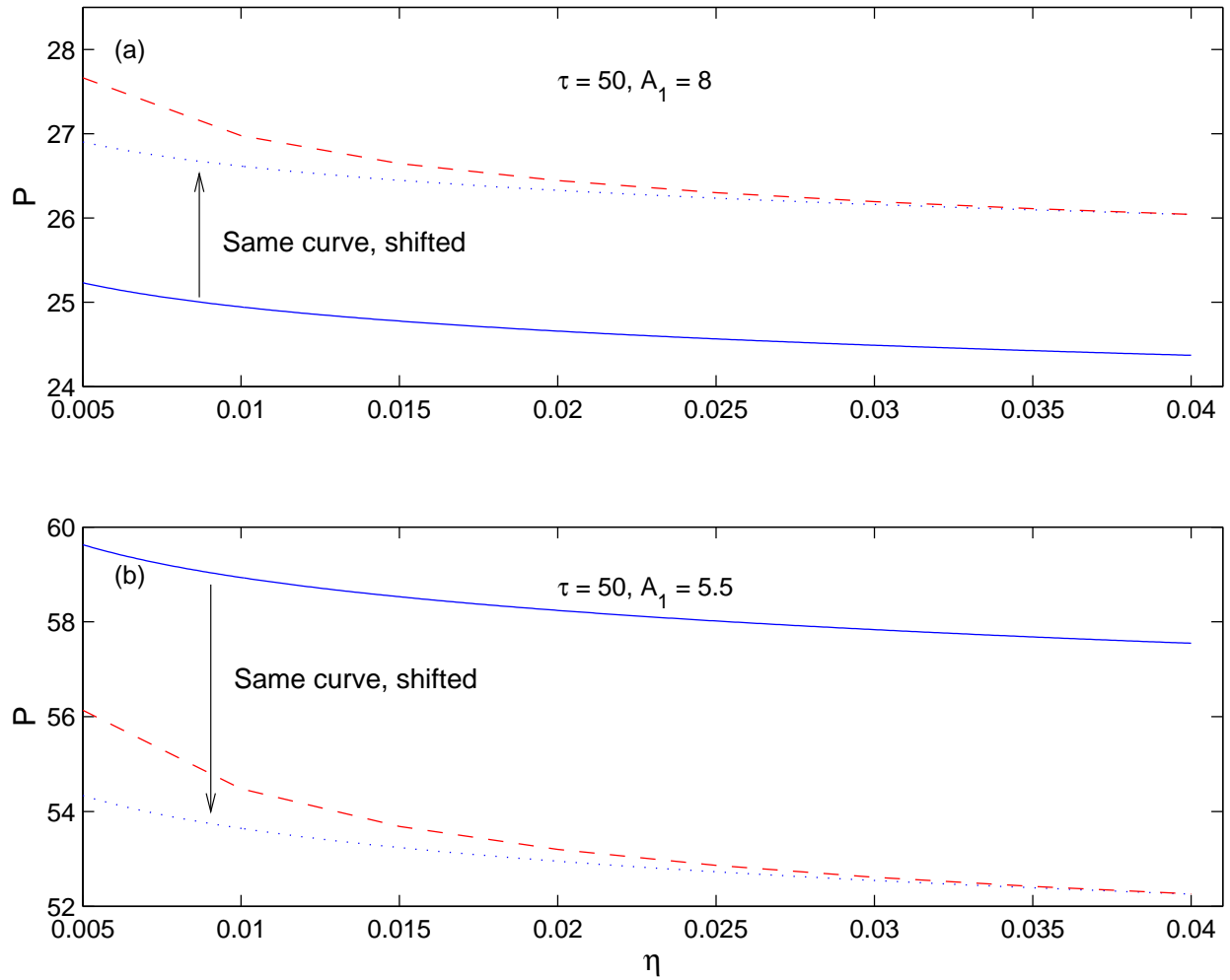


Figure 5: Period as a function of the feedback strength  $\eta$  for two different values of the pump. Solid curves = analytical, dashed = numerical.

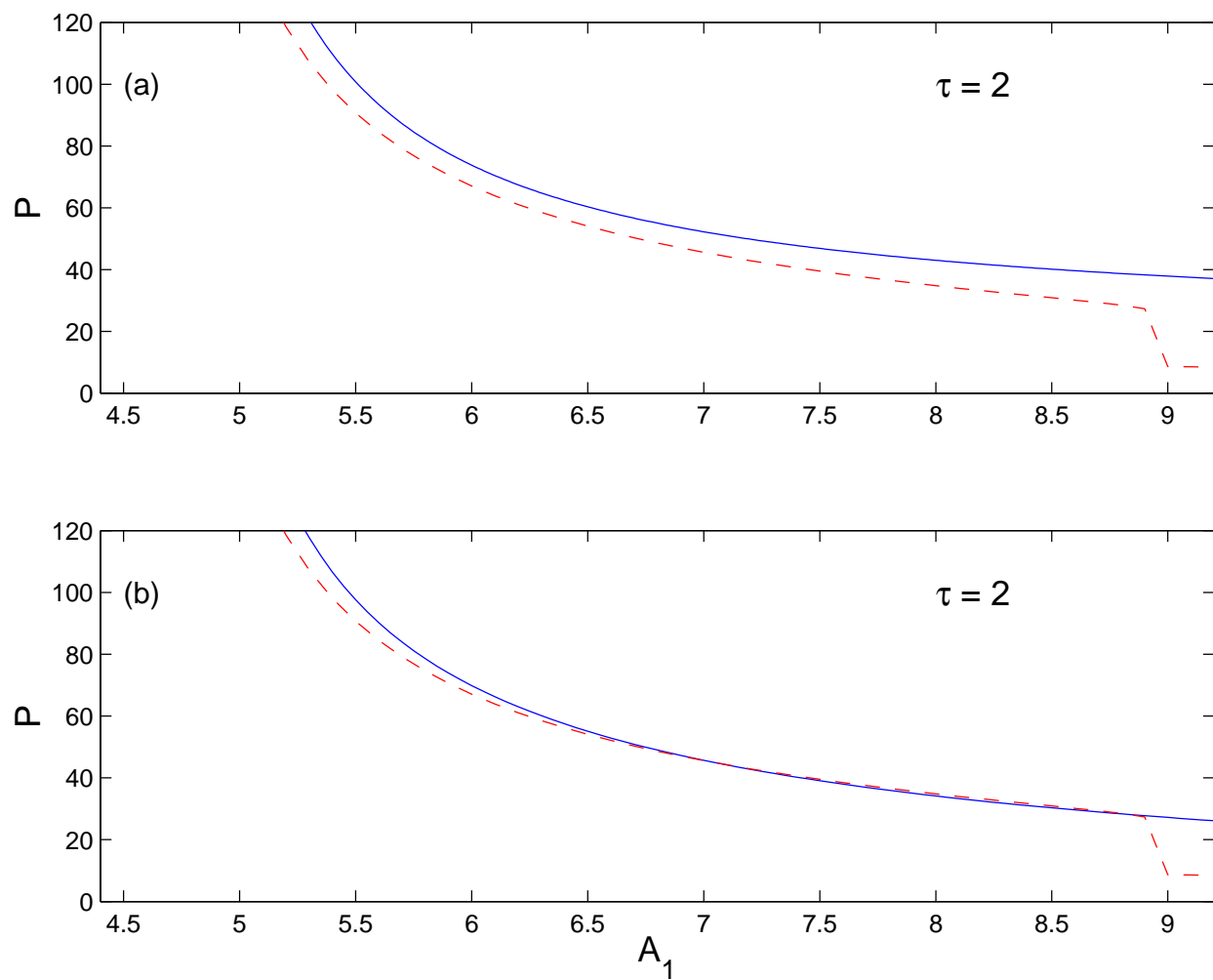


Figure 6: For short delay the period is shifted from the  $\eta = 0$  curve. The period does not become small enough before the upper Hopf bifurcation to lock to an integer fraction of the delay. Solid curves = analytical, dashed = numerical.

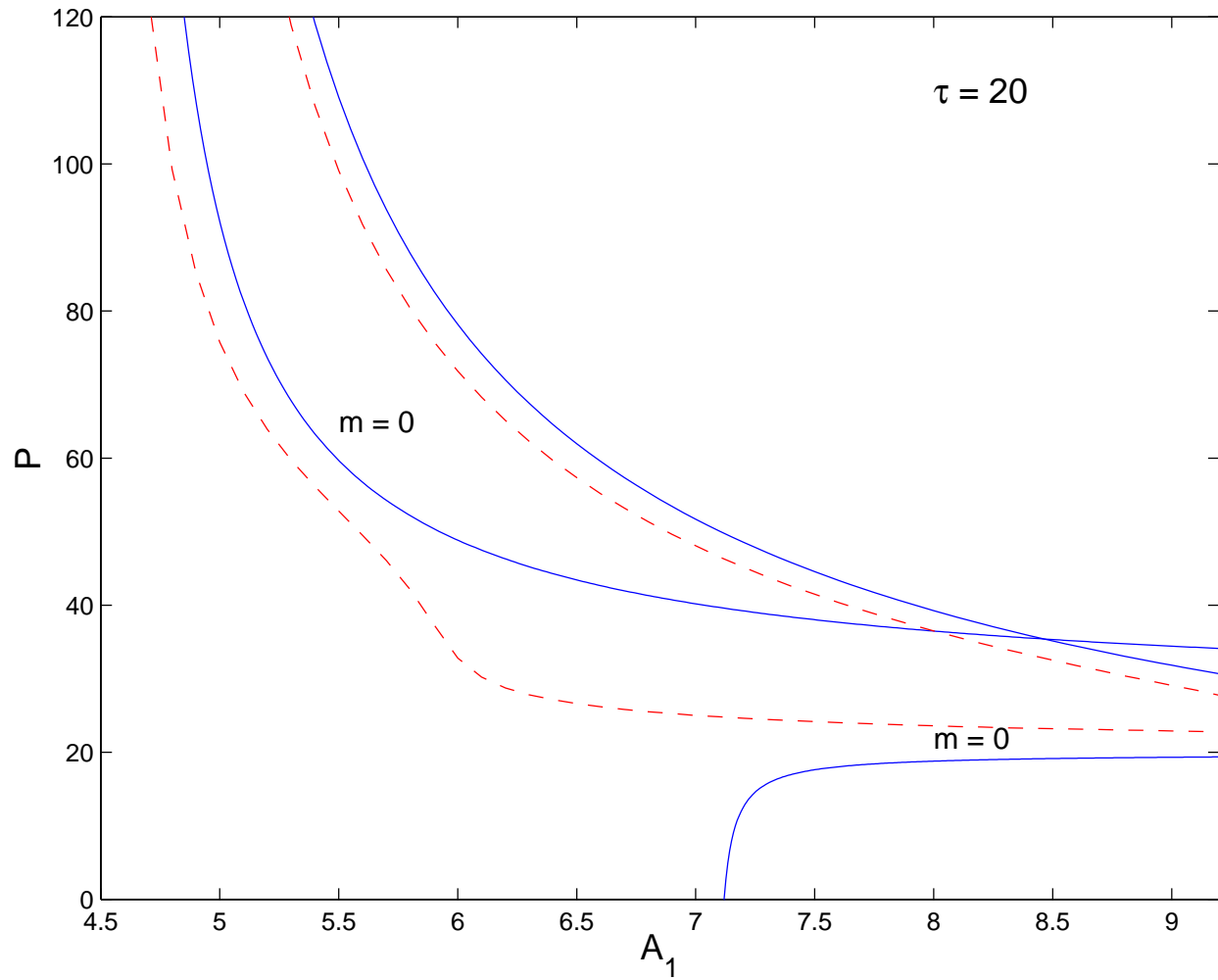


Figure 7: For moderate delays the period first decays as the pump is increased and then abruptly drops to the  $m = 0$  locked state. Solid curves = analytical, dashed = numerical.